CORE
Metadata, citation and similar papers at core.ac.uk
Provided by Elsevier - Publisher Connector

ELSEVIER

Available online at www.sciencedirect.com
ScienceDirect

J. Math. Anal. Appl. 331 (2007) 547–566

Journal of MATHEMATICAL ANALYSIS AND APPLICATIONS

www.elsevier.com/locate/jmaa

A study of type I intermittency of a circular differential equation under a discontinuous right-hand side ☆

Chein-Shan Liu

Department of Mechanical and Mechatronic Engineering, Taiwan Ocean University, Keelung, Taiwan

Received 15 December 2004

Available online 5 October 2006

Submitted by C. Simó

Abstract

In this paper we study a circular differential equation under a discontinuous periodic input, developing a quadratic differential equations system on $\mathbb{S}^1$ and a linear differential equations system in the Minkowski space $\mathbb{M}^3$. The symmetry groups of these two systems are, respectively, $PSO_o(2,1)$ and $SO_o(2,1)$. The Poincaré circle map is constructed exactly, and a critical value α_c of the parameter is identified. Depending on α of the input amplitude the equation may exhibit periodic, subharmonic or quasiperiodic motions. When α varies from $\alpha > \alpha_c$ to $\alpha < \alpha_c$, there undergoes an inverse tangent bifurcation; consequently, the resultant Poincaré circle map offers one route to the quasiperiodicity via a type I intermittency. In the parameter range of $\alpha < \alpha_c$ the orbit generated by the Poincaré circle map is either m-periodic or quasiperiodic when n/m is a rational or an irrational number.
© 2006 Elsevier Inc. All rights reserved.

Keywords: Circular differential equation; Intermittency; Quasiperiodicity; Poincaré circle map; Inverse tangent bifurcation; Lorentz group

1. Introduction

The intermittency as that coined by Pomeau and Manneville [15] means the occurrence of a signal which alternates randomly between long regular phases and relatively short irregular bursts. It has also been observed that the intermittency offers a continuous route from regular to chaotic motion [17]. Recently, Wang and He [19] have developed a signal detection and estimation method based on the intermittency transition between order and chaos.

☆ The research was sponsored by the National Science Council of Taiwan under the grant NSC 95-2221-E-019-002.
E-mail address: csliu@mail.ntou.edu.tw.

0022-247X/$ – see front matter © 2006 Elsevier Inc. All rights reserved.
doi:10.1016/j.jmaa.2006.09.017

In this paper, we begin with the following circular differential equation:

$$\dot{\theta} = \|\dot{\mathbf{q}}\| \cos(\theta + \omega), \tag{1}$$

where

$$\|\dot{\mathbf{q}}\| := \sqrt{\dot{q}_1^2 + \dot{q}_2^2}, \qquad \omega := \arctan \frac{\dot{q}_1}{\dot{q}_2} \tag{2}$$

represent, respectively, the Euclidean norm and phase of $\dot{\mathbf{q}}$, which has two independent components $\dot{q}_1$ and $\dot{q}_2$ as nonzero inputs on the system. In Eq. (1), ω is an argument of $\dot{\mathbf{q}}$, where a dot stands for the time differentiation, and θ is a polar coordinate on $\mathbb{S}^1$.

Equation (1) may be encountered in the study of plasticity [8,9], double slip model of polycrystal plasticity [2,16], orientation dependent microfluid [3,5,18], and planar contact friction [13,14].

Equation (1) with $\dot{q}_1 = -\beta w \sin wt$, $\dot{q}_2 = \beta w \cos wt$ and constant β and w:

$$\dot{\theta} = \beta w \cos(\theta - wt) \tag{3}$$

has been studied by Liu [6]. Depending on β the above equation may exhibit limit cycles, subharmonic or quasiperiodic motions. When β varies from $\beta > 1$ to $\beta < 1$, there undergoes an inverse tangent bifurcation and the resultant map offers one possible route to quasiperiodicity via type I intermittency. Liu [6] also gave a theoretical proof that the length of the laminar phase obeys the law of inverse square root, and that the map in the limiting of intermittency is a universal map which coincides with the result obtained by the renormalization group approach of Feigenbaum.

A further transformation of Eq. (3) by $x = (\theta - wt + \pi/2)/(2\pi)$, $a = -w/(2\pi)$ and $b = \beta w/(2\pi)$ leads to

$$\dot{x} = a + b \sin(2\pi x). \tag{4}$$

In Ref. [1] the above equation has been discretized by the Euler scheme with a step size h to a standard circle map:

$$x_{n+1} = \omega + x_n + \frac{\varepsilon}{2\pi} \sin(2\pi x_n), \tag{5}$$

where $\omega = ah$ and $\varepsilon = 2\pi bh$. The structure of the so-called Arnold tongues of the rational rotation is discussed in detail by Hale and Kocak in Ref. [1].

Equation (1) with a discontinuous right-hand side however is not yet studied in the literature. In this paper, we extend the previous studies [6,8] by allowing $\dot{\mathbf{q}}$ to be a discontinuous function of time and extend the results in [11] to a larger extent by considering the long term behavior and its bifurcation. This paper is organized as follows. We transform Eq. (1) to a quadratic nonlinear differential equations system on $\mathbb{S}^1$ and exactly linearize them in the three-dimensional Minkowski space $\mathbb{M}^3$ in Section 2. In Section 3 we characterize that the internal symmetry of the considered system is a Lorentz group $SO_o(2,1)$, and the circle map basing on the group is developed. In Section 4 we start to consider a discontinuous periodic input exerted on the system, of which the closed-form solution is derived. Moreover, the long term behavior is studied in Section 5 via the technique of Poincaré circle map. We prove that the control parameter α of input amplitude plays a key role to shape the main characters of the system behavior in Section 6. When α varies from $\alpha > \alpha_c$ to $\alpha < \alpha_c$ the transition from a periodic motion to a quasiperiodic motion is characterized by an inverse tangent bifurcation in which two fixed points (a stable and an unstable) merge together, and after that a type I intermittency appears. Then, one way of intermittency to quasiperiodicity is identified in Section 7. Finally, we draw some conclusions in Section 8.

2. Exact linearization

Upon considering

$$(x, y) := (\cos\theta, \sin\theta) \tag{6}$$

as a point on $\mathbb{S}^1$, from Eq. (1) one has

$$\dot{x} = -\|\dot{\mathbf{q}}\| \sin\theta[\cos\theta\cos\omega - \sin\theta\sin\omega], \tag{7}$$

$$\dot{y} = \|\dot{\mathbf{q}}\| \cos\theta[\cos\theta\cos\omega - \sin\theta\sin\omega], \tag{8}$$

which, with the aid of Eq. (2), can be recast to

$$\dot{x} = -xy\dot{q}_2 - x^2\dot{q}_1 + \dot{q}_1, \tag{9}$$

$$\dot{y} = -xy\dot{q}_1 - y^2\dot{q}_2 + \dot{q}_2. \tag{10}$$

We thus have two coupled quadratic differential equations on $\mathbb{S}^1$ under the external inputs $\dot{q}_1$ and $\dot{q}_2$.

By considering the integrating factor

$$X_0(t) := \exp\left[\int_0^t x(\zeta)\dot{q}_1(\zeta) + y(\zeta)\dot{q}_2(\zeta)\right] d\zeta, \tag{11}$$

Eqs. (9) and (10) become

$$\frac{d}{dt}(X_0 x) = X_0\dot{q}_1, \tag{12}$$

$$\frac{d}{dt}(X_0 y) = X_0\dot{q}_2. \tag{13}$$

Furthermore, from Eqs. (11), (6) and (2) it follows that

$$\dot{X}_0 = X_0 x\dot{q}_1 + X_0 y\dot{q}_2 = \|\dot{\mathbf{q}}\| X_0 \sin(\theta + \omega). \tag{14}$$

Upon introducing

$$\mathbf{X} = \begin{bmatrix} X_1 \\ X_2 \\ X_0 \end{bmatrix} := \begin{bmatrix} X_0 x \\ X_0 y \\ X_0 \end{bmatrix} \tag{15}$$

and putting Eqs. (12)–(14) together we obtain

$$\dot{\mathbf{X}} = \mathbf{A}\mathbf{X}, \tag{16}$$

where

$$\mathbf{A} := \begin{bmatrix} 0 & 0 & \dot{q}_1 \\ 0 & 0 & \dot{q}_2 \\ \dot{q}_1 & \dot{q}_2 & 0 \end{bmatrix}. \tag{17}$$

Due to $x^2 + y^2 = 1$ the three variables X_1, X_2 and X_0 fulfill the cone condition:

$$X_1^2 + X_2^2 - X_0^2 = 0. \tag{18}$$

$\mathbf{X}$ is a point in the three-dimensional Minkowski space $\mathbb{M}^3$, that is, $\mathbf{X} = (X_0 x, X_0 y, X_0)^{\mathrm{T}} \in \mathbb{M}^3$. Throughout this paper the superscript T denotes the transpose. Up to here, the circular differential equation (1) has been transformed into a more tractable linear equation (16).

3. Lorentz group $SO_o(2,1)$

From Eq. (17) it is easy to check that the matrix $\mathbf{A}$ satisfies

$$\mathbf{A}^{\mathrm{T}}\mathbf{g} + \mathbf{g}\mathbf{A} = \mathbf{0}, \tag{19}$$

where

$$\mathbf{g} := \begin{bmatrix} 1 & 0 & 0 \\ 0 & 1 & 0 \\ 0 & 0 & -1 \end{bmatrix} \tag{20}$$

is a metric tensor of $\mathbb{M}^3$. So $\mathbf{A}$ is an element of the real Lie algebra $so(2,1)$ of the Lorentz group $SO_o(2,1)$.

The Lorentz group $SO_o(2,1) \ni \mathbf{G}$ is the group composed of all linear transformations in the Minkowski space $\mathbb{M}^3$ which render the Minkowski separation $X_1^2 + X_2^2 - X_0^2$ invariant:

$$\mathbf{G}^{\mathrm{T}}\mathbf{g}\mathbf{G} = \mathbf{g}. \tag{21}$$

If the initial point $\mathbf{X}(0)$ is already located on the cone then the subsequent point $\mathbf{X}(t)$ will remain on the cone by the following transformation:

$$\mathbf{X}(t) = \mathbf{G}(t)\mathbf{X}(0). \tag{22}$$

By Eqs. (22) and (15) we have

$$X_0(t)\begin{bmatrix} x(t) & y(t) & 1 \end{bmatrix}^{\mathrm{T}} = X_0(0)\mathbf{G}(t)\begin{bmatrix} x(0) & y(0) & 1 \end{bmatrix}^{\mathrm{T}}. \tag{23}$$

Through some manipulations we thus obtain

$$x(t) = \frac{G_{11}x(0) + G_{12}y(0) + G_{13}}{G_{31}x(0) + G_{32}y(0) + G_{33}}, \tag{24}$$

$$y(t) = \frac{G_{21}x(0) + G_{22}y(0) + G_{23}}{G_{31}x(0) + G_{32}y(0) + G_{33}}. \tag{25}$$

Corresponding to the symmetry group $\mathbf{G}$ of Eq. (16), the symmetry group of Eqs. (9) and (10) as presented by the above two equations is a projection of $\mathbf{G}$ denoted by $PSO_o(2,1)$.

Taking the sum of the squares of above $x(t)$ and $y(t)$ and using the formula in Eq. (21) we can obtain

$$x^2(t) + y^2(t) = \frac{x^2(0) + y^2(0) - 1 + [G_{31}x(0) + G_{32}y(0) + G_{33}]^2}{[G_{31}x(0) + G_{32}y(0) + G_{33}]^2}. \tag{26}$$

It is straightforward to show that $x^2(t) + y^2(t) = 1$ when $x^2(0) + y^2(0) = 1$. In this sense Eqs. (24) and (25) are circle mapping, which map the point in the unit circle to another point in the unit circle, leaving the unit circle invariant.

The transformation from the group $SL(2,\mathbb{R})$ onto the group $SO_o(2,1)$ is a *spinor map*. Liu and Hong [12] have developed an effective algebraic procedure to construct the spinor map from $SL(2,\mathbb{R})$ onto $SO_o(2,1)$, $SL(2,\mathbb{C})$ onto $SO_o(3,1)$ and also $SL(2,\mathbb{H})$ onto $SO_o(5,1)$, where $\mathbb{H}$ is a quaternion field. The last result as advocated by Liu [10] is very useful in the computational plasticity of large deformation models.

4. A discontinuous periodic input

The results as shown in the previous two sections are applicable in general for any input on the system. However, in order to investigate the periodic behavior of the system under a discontinuous input more succinctly, we specialize the input into a certain form.

When Eqs. (9) and (10) are subjected to a constant two-dimensional vector $\dot{\mathbf{q}} = (\dot{q}_1, \dot{q}_2)$, the solutions of x and y by solving Eq. (16) are found to be [11]

$$x(t) = \frac{x(t_i) + \{C_1[e^{\|\dot{\mathbf{q}}\|(t-t_i)} - 1] + C_2[1 - e^{-\|\dot{\mathbf{q}}\|(t-t_i)}]\}\dot{q}_1/\|\dot{\mathbf{q}}\|}{C_1 e^{\|\dot{\mathbf{q}}\|(t-t_i)} + C_2 e^{-\|\dot{\mathbf{q}}\|(t-t_i)}}, \tag{27}$$

$$y(t) = \frac{y(t_i) + \{C_1[e^{\|\dot{\mathbf{q}}\|(t-t_i)} - 1] + C_2[1 - e^{-\|\dot{\mathbf{q}}\|(t-t_i)}]\}\dot{q}_2/\|\dot{\mathbf{q}}\|}{C_1 e^{\|\dot{\mathbf{q}}\|(t-t_i)} + C_2 e^{-\|\dot{\mathbf{q}}\|(t-t_i)}}, \tag{28}$$

which supply a nonlinear circle mapping from the initial values of $(x(t_i), y(t_i))$ specifying at an initial time $t = t_i$ to the current values of $(x(t), y(t))$ for all $t \geqslant t_i$. The above C_1 and C_2 are integration constants given by

$$C_1 := \frac{1}{2}\left[1 + x(t_i)\frac{\dot{q}_1}{\|\dot{\mathbf{q}}\|} + y(t_i)\frac{\dot{q}_2}{\|\dot{\mathbf{q}}\|}\right], \tag{29}$$

$$C_2 := \frac{1}{2}\left[1 - x(t_i)\frac{\dot{q}_1}{\|\dot{\mathbf{q}}\|} - y(t_i)\frac{\dot{q}_2}{\|\dot{\mathbf{q}}\|}\right]. \tag{30}$$

Hereafter, we consider a periodic square path with period T. In each side of the square path the length is α as shown in Fig. 1, and $\dot{q}_1$ and $\dot{q}_2$ are given by

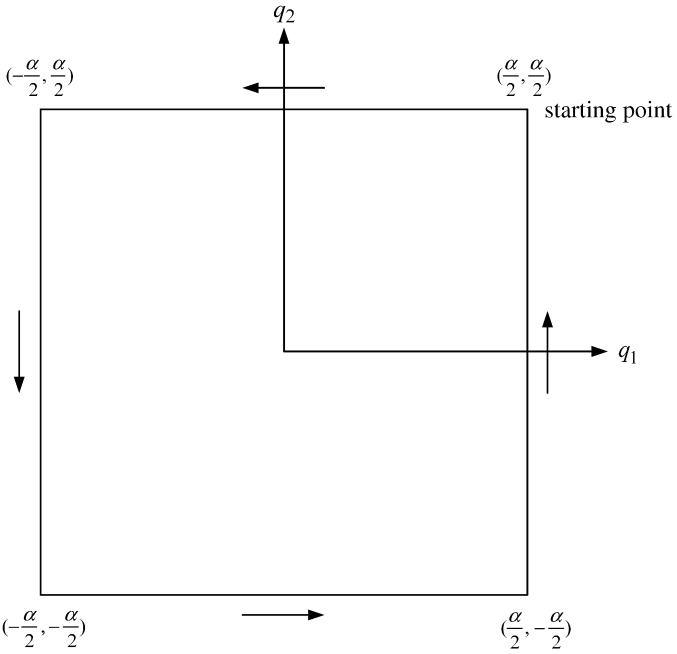

Fig. 1. The input path is a square in the plane (q_1, q_2) with length α of each side.

$$\dot{q}_1(t) = \begin{cases} \frac{-4\alpha}{T}, & 0 \leqslant t \bmod T < \frac{T}{4}, \\ 0, & \frac{T}{4} \leqslant t \bmod T < \frac{T}{2}, \\ \frac{4\alpha}{T}, & \frac{T}{2} \leqslant t \bmod T < \frac{3T}{4}, \\ 0, & \frac{3T}{4} \leqslant t \bmod T < T, \end{cases} \tag{31}$$

$$\dot{q}_2(t) = \begin{cases} 0, & 0 \leqslant t \bmod T < \frac{T}{4}, \\ \frac{-4\alpha}{T}, & \frac{T}{4} \leqslant t \bmod T < \frac{T}{2}, \\ 0, & \frac{T}{2} \leqslant t \bmod T < \frac{3T}{4}, \\ \frac{4\alpha}{T}, & \frac{3T}{4} \leqslant t \bmod T < T. \end{cases} \tag{32}$$

In the below, it will be seen that the input amplitude $\alpha > 0$ plays a key role to determine the behavior of Eq. (1) under the inputs of Eqs. (31) and (32).

5. Poincaré circle map

For the periodic path composed of the four straight lines as shown in Fig. 1 the speed term $\|\dot{\mathbf{q}}\|$ along each line has the same value $4\alpha/T$ as can be seen from Eqs. (31) and (32). Supposing that the system is subjected to the square path periodically, and that the starting point of (x, y) is located on the unit circle, what we attempt to know is the periodic behavior, which will be studied below by the technique of Poincaré map.

The one-period Poincaré map can be constructed as follows. While the starting (x, y) is assigned as $(x^{(1)}, y^{(1)})$, (x, y) at the end of the first branch of the input path is denoted by $(x^{(2)}, y^{(2)})$, subsequently by $(x^{(3)}, y^{(3)})$ and $(x^{(4)}, y^{(4)})$, and then at the end of one period input by $(x^{(5)}, y^{(5)})$.

In what follows we attempt to construct a periodic mapping between $(x^{(1)}, y^{(1)})$ and $(x^{(5)}, y^{(5)})$. For each branch of the periodic path the elapsed times $t_2 - t_1$, $t_3 - t_2$, $t_4 - t_3$ and $t_5 - t_4$ are all equal to $T/4$. Thus we set

$$\rho := e^{\alpha}, \quad 1 < \rho < \infty. \tag{33}$$

From Eqs. (27) and (28) we can derive the map from $(x^{(1)}, y^{(1)})$ to $(x^{(2)}, y^{(2)})$ as follows:

$$x^{(2)} = \frac{1}{\rho C_1 + \rho^{-1} C_2} \left\{ x^{(1)} + \left[(\rho - 1) C_1 + \left(1 - \rho^{-1}\right) C_2 \right] \frac{\dot{q}_1}{\|\dot{\mathbf{q}}\|} \right\}, \tag{34}$$

$$y^{(2)} = \frac{1}{\rho C_1 + \rho^{-1} C_2} \left\{ y^{(1)} + \left[(\rho - 1) C_1 + \left(1 - \rho^{-1}\right) C_2 \right] \frac{\dot{q}_2}{\|\dot{\mathbf{q}}\|} \right\}. \tag{35}$$

From Eqs. (29) and (30) with $x(t_i)$ replaced by $x^{(1)}$ and $y(t_i)$ by $y^{(1)}$ and by using Eqs. (31) and (32), the above C_1 and C_2 terms can be derived as follows:

$$C_1 = \frac{1}{2} - \frac{x^{(1)}}{2}, \tag{36}$$

$$C_2 = \frac{1}{2} + \frac{x^{(1)}}{2}. \tag{37}$$

By Eqs. (31), (32), (36) and (37), Eqs. (34) and (35) can be combined to a neater form:

$$\begin{bmatrix} x^{(2)} \\ y^{(2)} \end{bmatrix} = \frac{\begin{bmatrix} a & 0 \\ 0 & 1 \end{bmatrix} \begin{bmatrix} x^{(1)} \\ y^{(1)} \end{bmatrix} - \begin{bmatrix} b \\ 0 \end{bmatrix}}{\begin{bmatrix} -b & 0 \end{bmatrix} \begin{bmatrix} x^{(1)} \\ y^{(1)} \end{bmatrix} + a}, \tag{38}$$

where

$$a := \frac{1}{2}\left(\rho + \frac{1}{\rho}\right) = \cosh\alpha, \tag{39}$$

$$b := \frac{1}{2}\left(\rho - \frac{1}{\rho}\right) = \sinh\alpha. \tag{40}$$

Similarly, the other maps can be derived as follows:

$$\begin{bmatrix} x^{(3)} \\ y^{(3)} \end{bmatrix} = \frac{\begin{bmatrix} 1 & 0 \\ 0 & a \end{bmatrix}\begin{bmatrix} x^{(2)} \\ y^{(2)} \end{bmatrix} - \begin{bmatrix} 0 \\ b \end{bmatrix}}{\begin{bmatrix} 0 & -b \end{bmatrix}\begin{bmatrix} x^{(2)} \\ y^{(2)} \end{bmatrix} + a}, \tag{41}$$

$$\begin{bmatrix} x^{(4)} \\ y^{(4)} \end{bmatrix} = \frac{\begin{bmatrix} a & 0 \\ 0 & 1 \end{bmatrix}\begin{bmatrix} x^{(3)} \\ y^{(3)} \end{bmatrix} + \begin{bmatrix} b \\ 0 \end{bmatrix}}{\begin{bmatrix} b & 0 \end{bmatrix}\begin{bmatrix} x^{(3)} \\ y^{(3)} \end{bmatrix} + a}, \tag{42}$$

$$\begin{bmatrix} x^{(5)} \\ y^{(5)} \end{bmatrix} = \frac{\begin{bmatrix} 1 & 0 \\ 0 & a \end{bmatrix}\begin{bmatrix} x^{(4)} \\ y^{(4)} \end{bmatrix} + \begin{bmatrix} 0 \\ b \end{bmatrix}}{\begin{bmatrix} 0 & b \end{bmatrix}\begin{bmatrix} x^{(4)} \\ y^{(4)} \end{bmatrix} + a}. \tag{43}$$

While the substitution of Eq. (42) into (43) gives the map from $(x^{(3)}, y^{(3)})$ to $(x^{(5)}, y^{(5)})$,

$$\begin{bmatrix} x^{(5)} \\ y^{(5)} \end{bmatrix} = \frac{\begin{bmatrix} a & 0 \\ b^2 & a \end{bmatrix}\begin{bmatrix} x^{(3)} \\ y^{(3)} \end{bmatrix} + \begin{bmatrix} b \\ ab \end{bmatrix}}{\begin{bmatrix} ab & b \end{bmatrix}\begin{bmatrix} x^{(3)} \\ y^{(3)} \end{bmatrix} + a^2}, \tag{44}$$

the substitution of Eq. (38) into (41) gives the map from $(x^{(1)}, y^{(1)})$ to $(x^{(3)}, y^{(3)})$,

$$\begin{bmatrix} x^{(3)} \\ y^{(3)} \end{bmatrix} = \frac{\begin{bmatrix} a & 0 \\ b^2 & a \end{bmatrix}\begin{bmatrix} x^{(1)} \\ y^{(1)} \end{bmatrix} - \begin{bmatrix} b \\ ab \end{bmatrix}}{\begin{bmatrix} -ab & -b \end{bmatrix}\begin{bmatrix} x^{(1)} \\ y^{(1)} \end{bmatrix} + a^2}. \tag{45}$$

Finally, the substitution of Eq. (45) into (44) gives the map from $(x^{(1)}, y^{(1)})$ to $(x^{(5)}, y^{(5)})$,

$$\begin{bmatrix} x^{(5)} \\ y^{(5)} \end{bmatrix} = \frac{\begin{bmatrix} a^2-ab^2 & -b^2 \\ 2ab^2-a^2b^2 & a^2-ab^2 \end{bmatrix}\begin{bmatrix} x^{(1)} \\ y^{(1)} \end{bmatrix} + \begin{bmatrix} a^2b-ab \\ a^3b-a^2b-b^3 \end{bmatrix}}{\begin{bmatrix} -a^3b+a^2b+b^3 & -a^2b+ab \end{bmatrix}\begin{bmatrix} x^{(1)} \\ y^{(1)} \end{bmatrix} + a^4 - 2ab^2}. \tag{46}$$

The above map is a one-period Poincaré circle map. However, we use

$$\begin{bmatrix} x(n+1) \\ y(n+1) \end{bmatrix} = \frac{\begin{bmatrix} G_{11} & G_{12} \\ G_{21} & G_{22} \end{bmatrix}\begin{bmatrix} x(n) \\ y(n) \end{bmatrix} + \begin{bmatrix} G_{13} \\ G_{23} \end{bmatrix}}{\begin{bmatrix} G_{31} & G_{32} \end{bmatrix}\begin{bmatrix} x(n) \\ y(n) \end{bmatrix} + G_{33}}, \tag{47}$$

$n = 1, 2, 3, \ldots$, to denote the recursive Poincaré circle map, where

$$\mathbf{G} := \begin{bmatrix} G_{11} & G_{12} & G_{13} \\ G_{21} & G_{22} & G_{23} \\ G_{31} & G_{32} & G_{33} \end{bmatrix} = \begin{bmatrix} a^2 - ab^2 & -b^2 & a^2b - ab \\ 2ab^2 - a^2b^2 & a^2 - ab^2 & a^3b - a^2b - b^3 \\ a^2b + b^3 - a^3b & ab - a^2b & a^4 - 2ab^2 \end{bmatrix}. \tag{48}$$

In terms of the homogeneous coordinates $(X_0 x, X_0 y, X_0)$ introduced in Eq. (15), Eq. (47) can also be written as

$$\begin{bmatrix} X_0(n+1)x(n+1) \\ X_0(n+1)y(n+1) \\ X_0(n+1) \end{bmatrix} = \mathbf{G}\begin{bmatrix} X_0(n)x(n) \\ X_0(n)y(n) \\ X_0(n) \end{bmatrix}, \tag{49}$$

which is an affine map. On the other hand, when dividing the second row by the first row in Eq. (47) and utilizing Eq. (6) we obtain the Poincaré circle map of another form:

$$\tan\theta(n+1)=\frac{G_{21}\cos\theta(n)+G_{22}\sin\theta(n)+G_{23}}{G_{11}\cos\theta(n)+G_{12}\sin\theta(n)+G_{13}}. \tag{50}$$

The bifurcation analysis basing on this equation will be conducted in Section 7.

By the relation $a^2-b^2=1$ obtained from Eqs. (39) and (40), the $\mathbf{G}$ defined in Eq. (48) can be proved to satisfy the identity in Eq. (21). For this reason $\mathbf{G}$ is a one-parameter subgroup of the homogeneous Lorentz group $SO_o(2,1)$, where $\mathbf{G}$ is dependent on α through Eqs. (48), (39) and (40). See, e.g., Liu [7] for a further discussion of the Lorentz group.

By inspecting the $\mathbf{G}$ in Eq. (48) the following equalities hold:

$$G_{11}=G_{22},\qquad G_{13}=-G_{32},\qquad G_{23}=-G_{31}. \tag{51}$$

For the later use we also prove an important identity for $\mathbf{G}$:

$$(\operatorname{tr}\mathbf{G})^2-2\operatorname{tr}\mathbf{G}-\operatorname{tr}\mathbf{G}^2=0, \tag{52}$$

where $\operatorname{tr}\mathbf{G}$ denotes the trace of $\mathbf{G}$.

In terms of the components of $\mathbf{G}$ the above equation is equivalent to

$$\begin{aligned}&(G_{11}+G_{22}+G_{33})^2-2(G_{11}+G_{22}+G_{33})\\&\quad-\left(G_{11}^2+G_{22}^2+G_{33}^2+2G_{12}G_{21}+2G_{13}G_{31}+2G_{23}G_{32}\right)=0.\end{aligned} \tag{53}$$

With the aid of Eq. (51) we need to prove

$$2G_{11}^2+4G_{11}G_{33}-4G_{11}-2G_{33}-2G_{12}G_{21}+4G_{31}G_{32}=0. \tag{54}$$

Substituting Eq. (48) for each component in the above equation we obtain

$$\begin{aligned}&2G_{11}^2+4G_{11}G_{33}-4G_{11}-2G_{33}-2G_{12}G_{21}+4G_{31}G_{32}\\&\quad=-8a^3b^2+4a^2b^4+4a^6-4a^2+8ab^2+8ab^4-8a^4b^2.\end{aligned} \tag{55}$$

Inserting $b^2=a^2-1$ and $b^4=a^4-2a^2+1$ we thus prove Eq. (54), and hence Eq. (52) holds.

6. Periodic orbit and bifurcation

The fixed point of the map (47) can be obtained by solving

$$\frac{\begin{bmatrix}G_{11}&G_{12}\\G_{21}&G_{22}\end{bmatrix}\begin{bmatrix}x\\y\end{bmatrix}+\begin{bmatrix}G_{13}\\G_{23}\end{bmatrix}}{\begin{bmatrix}G_{31}&G_{32}\end{bmatrix}\begin{bmatrix}x\\y\end{bmatrix}+G_{33}}=\begin{bmatrix}x\\y\end{bmatrix}. \tag{56}$$

Under the following transformation:

$$\eta:=G_{31}x+G_{32}y+G_{33}, \tag{57}$$

or

$$y=\frac{1}{G_{32}}(\eta-G_{31}x-G_{33}) \tag{58}$$

due to $G_{32}<0$, Eq. (56) changes to

$$x\eta = G_{11}x + \frac{G_{12}}{G_{32}}(\eta - G_{31}x - G_{33}) + G_{13}, \tag{59}$$

$$\frac{\eta}{G_{32}}(\eta - G_{31}x - G_{33}) = G_{21}x + \frac{G_{22}}{G_{32}}(\eta - G_{31}x - G_{33}) + G_{23}. \tag{60}$$

Substituting the first equation for $x\eta$ into the second one and cancelling the terms $G_{31}G_{11}x$ and $G_{31}G_{22}x$ on both the left and right sides due to $G_{11} = G_{22}$, we obtain

$$\eta^2 = d_1\eta + d_2x + d_3, \tag{61}$$

where

$$d_1 := \frac{G_{12}G_{31}}{G_{32}} + G_{22} + G_{33}, \tag{62}$$

$$d_2 := G_{21}G_{32} - \frac{G_{12}G_{31}^2}{G_{32}}, \tag{63}$$

$$d_3 := G_{13}G_{31} - \frac{G_{12}G_{31}G_{33}}{G_{32}} + G_{23}G_{32} - G_{22}G_{33}. \tag{64}$$

From Eq. (59) it follows that

$$x = \frac{G_{12}\eta - G_{12}G_{33} + G_{13}G_{32}}{G_{32}\eta - G_{11}G_{32} + G_{12}G_{31}}, \tag{65}$$

substituting which into Eq. (61) and then through some tedious calculations, we can get

$$\eta^3 - \operatorname{tr}\mathbf{G}\eta^2 + \frac{1}{2}\big[(\operatorname{tr}\mathbf{G})^2 - \operatorname{tr}\mathbf{G}^2\big]\eta - \det\mathbf{G} = 0, \tag{66}$$

where $\det\mathbf{G} = 1$ by Eq. (21).

For the cubic equation (66) there exists at least one real root given by

$$\eta = \frac{(\operatorname{tr}\mathbf{G})^2 - \operatorname{tr}\mathbf{G}^2}{2\operatorname{tr}\mathbf{G}} = 1. \tag{67}$$

We prove it with the aid of Eq. (52), from which the above second equality follows. Inserting $\eta = 1$ into Eq. (66) and noting $\det\mathbf{G} = 1$, it follows that Eq. (66) with $\eta = 1$ is identical to Eq. (52); hence, we prove that η given by Eq. (67) is a real root of Eq. (66).

Since $\eta = 1$ is a real root of Eq. (66) we can decompose it into

$$\big[\eta^2 + (1 - \operatorname{tr}\mathbf{G})\eta + 1\big](\eta - 1) = 0. \tag{68}$$

According to the value of the discriminant

$$\delta := (1 - \operatorname{tr}\mathbf{G})^2 - 4, \tag{69}$$

the number of the real roots of Eq. (66) are three for $\delta > 0$, two for $\delta = 0$ and one for $\delta < 0$.

For the cases of $\delta > 0$ the three real roots are given by

$$\eta_1 = \frac{\operatorname{tr}\mathbf{G} - 1 + \sqrt{(1 - \operatorname{tr}\mathbf{G})^2 - 4}}{2}, \tag{70}$$

$$\eta_2 = \frac{\operatorname{tr}\mathbf{G} - 1 - \sqrt{(1 - \operatorname{tr}\mathbf{G})^2 - 4}}{2}, \tag{71}$$

$$\eta_3 = \frac{(\operatorname{tr}\mathbf{G})^2 - \operatorname{tr}\mathbf{G}^2}{2\operatorname{tr}\mathbf{G}} = 1. \tag{72}$$

For the case $\delta = 0$ the two real roots are given by

$$\eta_1 = \eta_2 = \frac{\operatorname{tr}\mathbf{G} - 1}{2}, \qquad \eta_3 = \frac{(\operatorname{tr}\mathbf{G})^2 - \operatorname{tr}\mathbf{G}^2}{2\operatorname{tr}\mathbf{G}} = 1. \tag{73}$$

It will be shown later that $\eta_1 = \eta_2 = \eta_3 = 1$ because of $\operatorname{tr}\mathbf{G} = 3$ for $\delta = 0$.

For the cases of $\delta < 0$ the only one real root is given by

$$\eta = \frac{(\operatorname{tr}\mathbf{G})^2 - \operatorname{tr}\mathbf{G}^2}{2\operatorname{tr}\mathbf{G}} = 1. \tag{74}$$

The solution of $\delta = 0$ with δ given by Eq. (69) can be obtained analytically by solving

$$(1 - \operatorname{tr}\mathbf{G})^2 - 4 = 0. \tag{75}$$

From Eqs. (75) and (48) and $b^2 = a^2 - 1$ we obtain

$$a^4 - 4a^3 + 2a^2 + 4a - 3 = \left(a^2 - 4a + 3\right)\left(a^2 - 1\right) = 0. \tag{76}$$

Because of $a > 1$ due to Eq. (39), the only solution of the above equation is $a = 3$, and at the same time $\operatorname{tr}\mathbf{G} = 3$. The value of $a = 3$ can be expressed in terms of ρ by Eq. (39), which is a critical value denoted by $\rho_c = 3 + 2\sqrt{2}$ or $\alpha_c = \ln\rho_c = \ln(3 + 2\sqrt{2}) \approx 1.762747$ by Eq. (33). Substituting η into Eq. (65) we obtain x, and then substituting η and x into Eq. (58) we obtain y. In Fig. 2(a) we plot the point (x, y) for α in the range of $2 \geqslant \alpha \geqslant 1.6$.

We have numerically identified that when $\delta > 0$ ($\alpha > \alpha_c$) the (x, y) points generating from η_1 and η_2 locate on the unit circle and therefore are fixed points on the unit circle, and that the (x, y) points generating from η_3 are not the fixed points, because they are outside the unit circle. When α decreases to the critical value α_c, i.e. $\delta = 0$, the three curves merge at one point $(x_f, y_f) = (\sqrt{2}/2, \sqrt{2}/2)$ as shown in Fig. 2(a). The above values of (x_f, y_f) are calculated from Eqs. (65) and (58) with $\eta = 1$ and $a = 3$ and $b = 2\sqrt{2}$ for the related components of $\mathbf{G}$ as defined in Eq. (48). After that δ enters into the region $\delta < 0$ and there emerges one short curve marked by $\delta < 0$ in Fig. 2(a). By the same reason the (x, y) points in this curve are not the fixed points of the circle map (47) because this curve locates inside the unit circle. Therefore, when α varies from $\alpha > \alpha_c$ to $\alpha < \alpha_c$, the fixed points disappear.

The stability of fixed points can be investigated by considering the Jacobian matrix

$$\mathbf{J} := \begin{bmatrix} \frac{\partial J_1}{\partial x} & \frac{\partial J_1}{\partial y} \\ \frac{\partial J_2}{\partial x} & \frac{\partial J_2}{\partial y} \end{bmatrix} \tag{77}$$

of the maps

$$J_1(x, y) = \frac{G_{11}x + G_{12}y + G_{13}}{G_{31}x + G_{32}y + G_{33}}, \tag{78}$$

$$J_2(x, y) = \frac{G_{21}x + G_{22}y + G_{23}}{G_{31}x + G_{32}y + G_{33}}, \tag{79}$$

which are the right-hand side of Eq. (47). Substituting Eqs. (78) and (79) into Eq. (77), and calculating them in terms of (x, η) by Eq. (58) the following result is available:

$$\mathbf{J} = \frac{1}{G_{32}\eta} \begin{bmatrix} G_{32}(G_{11} - G_{31}x) & G_{32}(G_{12} - G_{32}x) \\ -G_{31}\eta + G_{31}^2 x + G_{21}G_{32} + G_{31}G_{33} & G_{32}(G_{31}x + G_{22} + G_{33} - \eta) \end{bmatrix}. \tag{80}$$

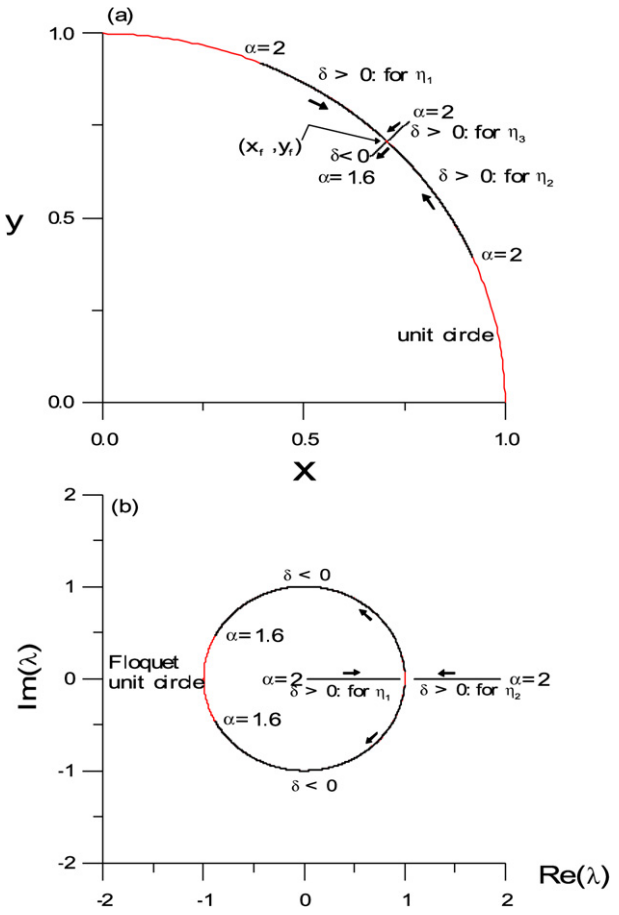

Fig. 2. In the parameter range of $2 \geqslant \alpha \geqslant 1.6$ the curves composed of fixed points are plotted in (a) and the corresponding eigenvalues of the Jacobian matrix are plotted in (b). The short arrows indicate the direction of α decreasing.

The eigenvalues for $\mathbf{J}$ are calculated by

$$\lambda^2 - \frac{\operatorname{tr}\mathbf{G} - \eta}{\eta}\lambda + \frac{\Gamma}{G_{32}\eta^2} = 0, \tag{81}$$

where

$$\begin{aligned}\Gamma := G_{32}\eta^2 \det \mathbf{J} = \left(G_{21}G_{32}^2 - G_{12}G_{31}^2\right)x - (G_{11}G_{32} - G_{12}G_{31})\eta + G_{11}G_{32}G_{22} \\ + G_{11}G_{32}G_{33} - G_{12}G_{21}G_{32} - G_{12}G_{31}G_{33}.\end{aligned} \tag{82}$$

Inserting Eq. (61) for x into the above equation we obtain

$$\Gamma := G_{32}\left[\eta^2 - \eta \operatorname{tr}\mathbf{G} + \frac{1}{2}(\operatorname{tr}\mathbf{G})^2 - \frac{1}{2}\operatorname{tr}\mathbf{G}^2\right]. \tag{83}$$

For the cases of $\delta > 0$ ($\alpha > \alpha_c$) the eigenvalues are given by

$$\lambda = \frac{\frac{\operatorname{tr}\mathbf{G}-\eta}{\eta} \pm \sqrt{(\frac{\operatorname{tr}\mathbf{G}-\eta}{\eta})^2 - \frac{4\Gamma}{G_{32}\eta^2}}}{2}, \tag{84}$$

where

$$\left(\frac{\operatorname{tr}\mathbf{G}-\eta}{\eta}\right)^2-\frac{4\Gamma}{G_{32}\eta^2}>0$$

was identified numerically. The eigenvalues with η_1 are both positive and smaller than 1, and the fixed point (x, y) is a sink. The eigenvalues with η_2 are both positive and greater than 1, and the fixed point (x, y) is a source. The eigenvalues with η_3 are both positive with one smaller than 1 and the other one greater than 1, and hence (x, y) is a saddle point. However, (x, y) generating from η_3 is not a fixed point on the unit circle as demonstrated above.

For the cases of $\delta<0$ ($\alpha<\alpha_c$) the eigenvalues are given by

$$\lambda=\frac{\operatorname{tr}\mathbf{G}-1\pm i\sqrt{4-(1-\operatorname{tr}\mathbf{G})^2}}{2}. \tag{85}$$

For these cases we have proved that the unique solution of Eq. (66) is $\eta=1$ as given by Eq. (74), which together with Eqs. (82) and (83) asserts that

$$\det\mathbf{J}=\frac{\Gamma}{G_{32}\eta^2}=\frac{\Gamma}{G_{32}}=1-\operatorname{tr}\mathbf{G}+\frac{1}{2}(\operatorname{tr}\mathbf{G})^2-\frac{1}{2}\operatorname{tr}\mathbf{G}^2=1. \tag{86}$$

The last equality is derived according to Eq. (52).

When δ varies from $\delta>0$ ($\alpha>\alpha_c$) to $\delta<0$ ($\alpha<\alpha_c$), a saddle-node bifurcation occurs at $\alpha=\alpha_c$, of which the eigenvalues pass through $+1$ in the Floquet unit circle, and jump to a pair of complex eigenvalues located on the unit circle, i.e. $|\lambda|=1$, as shown in Fig. 2(b). For the cases of $\delta>0$ we can see that the eigenvalues for the fixed points (x, y) generating from η_1 are both smaller than 1, whereas the eigenvalues for the fixed points (x, y) generating from η_2 are both greater than 1. The fixed points generating from η_1 are stable, and that generating from η_2 are unstable. In Fig. 3 we show a numerical iteration map with $\alpha=1.77$, the starting point of which is $(x, y)=(\cos\pi/6, -\sin\pi/6)$. It can be seen that the orbit tends to the stable fixed point very fast within only few steps as shown in Fig. 3(a); the variations of x and y with respect to N, which denotes the number of steps, are also plotted in Figs. 3(b) and 3(c).

For the cases of $\delta<0$ ($\alpha<\alpha_c$), the orbit generated by the map (47) is shown in Fig. 4, where we show a numerical iteration map with $\alpha=1$, the starting point of which is $(x, y)=(\cos 4\pi/9, \sin 4\pi/9)$. It can be seen that the orbit rotates on the unit circle and not tends to any fixed point as shown in Fig. 4(a); the variations of x and y with respect to N are plotted in Figs. 4(b) and 4(c).

From Eq. (85) it can be seen that

$$|\lambda|=1, \tag{87}$$

which means that there exists an angle ϕ, such that

$$\lambda=e^{i\phi}=\cos\phi+i\sin\phi. \tag{88}$$

As demonstrated by Kuznetsov [4] the parameter corresponding to a rational rotation number n/m is determined by

$$\lambda=e^{i\phi},\quad \phi=\frac{2n\pi}{m}. \tag{89}$$

Combining Eqs. (88) and (89) we thus can derive the following result. For the rational rotation with a rotation angle $2n\pi/m$, where $n<m$ and m, n are positive integers and primed relatively, the parameter can be determined by the following equation:

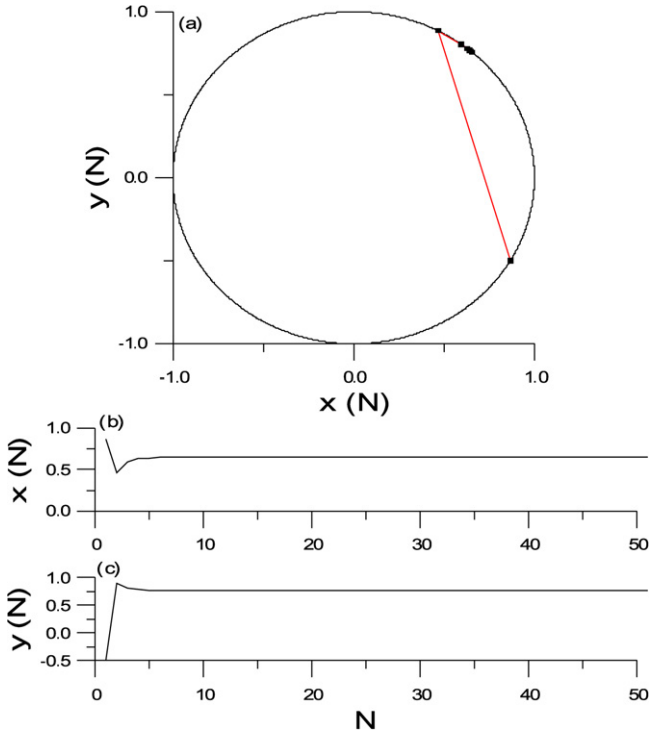

Fig. 3. For the case $\alpha = 1.77$ the iteration orbit of (x, y) is plotted in (a), and the variations of $x(N)$ and $y(N)$ with respect to N are plotted in (b) and (c).

$$\tan\left(\frac{2n\pi}{m}\right) = \frac{\sqrt{4-(1-\operatorname{tr}\mathbf{G})^2}}{\operatorname{tr}\mathbf{G}-1}, \tag{90}$$

of which the right-hand side is the ratio of the imaginary and real parts of the eigenvalue given in Eq. (85).

It is interesting to note that η satisfying Eq. (66) is also an eigenvalue of $\mathbf{G}$. In the cases of $\delta < 0$ ($\alpha < \alpha_c$), the first two eigenvalues η_1 and η_2 defined in Eqs. (70) and (71) are conjugate complex numbers. Upon comparing these two equations with Eq. (85), we can conclude that the λ defined by Eq. (85) are both the eigenvalues of $\mathbf{J}$ and $\mathbf{G}$ under the condition of $\delta < 0$ ($\alpha < \alpha_c$). Therefore, we have

$$\mathbf{G}\mathbf{X} = \lambda\mathbf{X}. \tag{91}$$

Suppose that the eigenvalue is of the form $\lambda = e^{2in\pi/m}$, and applying the above mapping m times leads to

$$\mathbf{G}^m\mathbf{X} = \lambda^m\mathbf{X} = e^{2in\pi}\mathbf{X} = \mathbf{X}. \tag{92}$$

It means that $\mathbf{X}$ is a m-periodic point. By using Eq. (15) through the projection of $\mathbf{X}$ into the unit circle, we thus can derive the following result. Suppose that $x + iy = e^{i\theta} \in \mathbb{S}^1$ is a point in the unit circle, and at that point the eigenvalue is of the form $\lambda = e^{2in\pi/m}$, then in the unit circle that point is a m-periodic point.

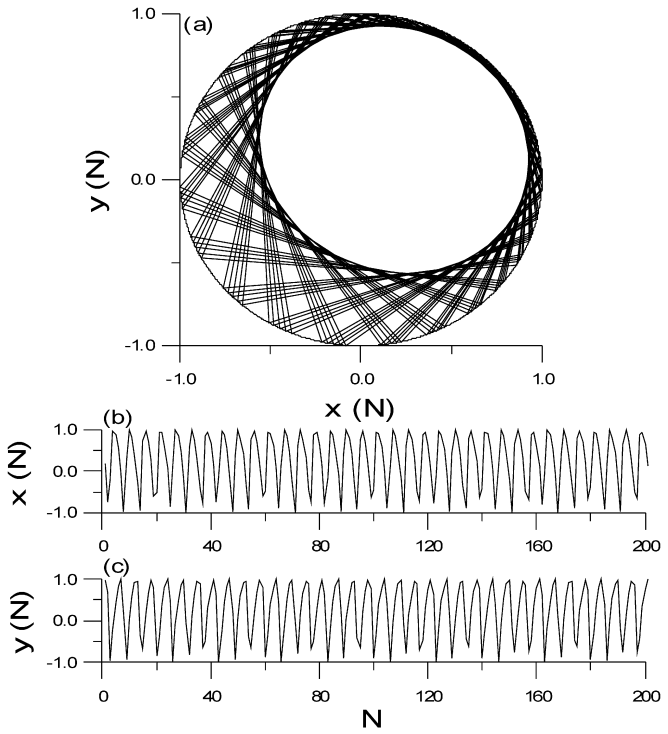

Fig. 4. For the case $\alpha = 1$ the iteration orbit of (x, y) is plotted in (a), and the variations of $x(N)$ and $y(N)$ with respect to N are plotted in (b) and (c).

After some manipulations of Eq. (90) we can get

$$\operatorname{tr}\mathbf{G} - \left[1 + 2\cos\left(\frac{2n\pi}{m}\right)\right] = 0, \tag{93}$$

which by Eq. (48) can be written as

$$a^4 - 4a^3 + 2a^2 + 4a - \left[1 + 2\cos\left(\frac{2n\pi}{m}\right)\right] = 0. \tag{94}$$

The solution of this equation gives the parameter a and thus α for the corresponding rational rotation n/m, and then all the points on the unit circle are m-periodic; otherwise, there are no points on the unit circle periodic, and indeed they are quasiperiodic.

Given $n/m = 1/2$ and $n/m = 1/3$ we solve Eq. (94) by the Newton–Raphson method, which gives the values about $\alpha = 1.528571$ and $\alpha = 1.316958$. Basing on these parameter values we calculate $x(t)$ and $y(t)$ by Eqs. (27) and (28), and $\dot{x}(t)$ and $\dot{y}(t)$ by Eqs. (9) and (10). The phase portraits of $(x, \dot{x})$ and $(y, \dot{y})$ for the above two cases are plotted in Figs. 5 and 6, respectively. We also plotted $(n_1, \dot{n}_1)$ and $(n_2, \dot{n}_2)$, where $n_1 = \cos(\theta/2)$ and $n_2 = \sin(\theta/2)$. It can be seen that they are respectively 1/2- and 1/3-subharmonic motions. In general, in the parameter range of $\delta < 0$ ($\alpha < \alpha_c$) the motion is quasiperiodic as shown in Fig. 7 with $\alpha = 1.5$. In these calculations the period $T = 1$ s, and the initial values of $\theta = 0$, i.e., $x = 1$ and $y = 0$ were fixed.

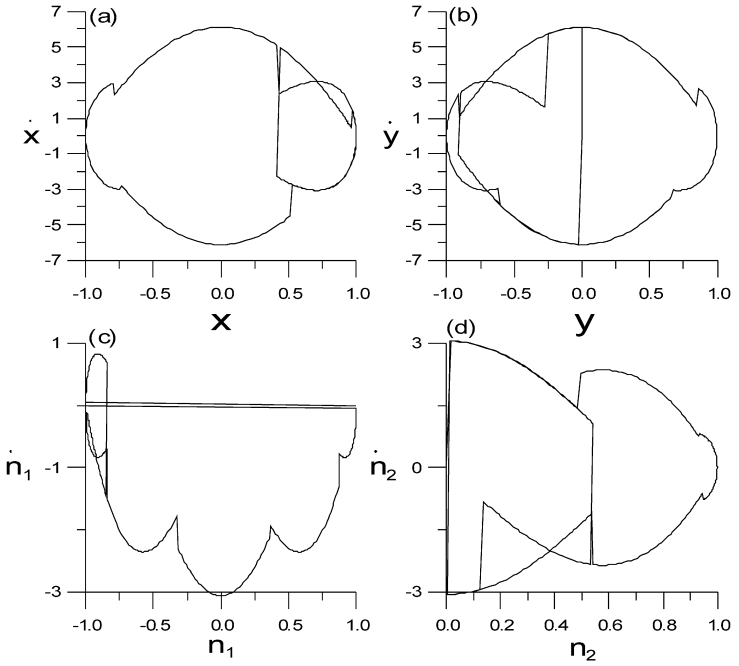

Fig. 5. The 1/2-subharmonic motion is shown through the phase portraits of (a) $(x, \dot{x})$, (b) $(y, \dot{y})$, (c) $(n_1, \dot{n}_1)$ and (d) $(n_2, \dot{n}_2)$.

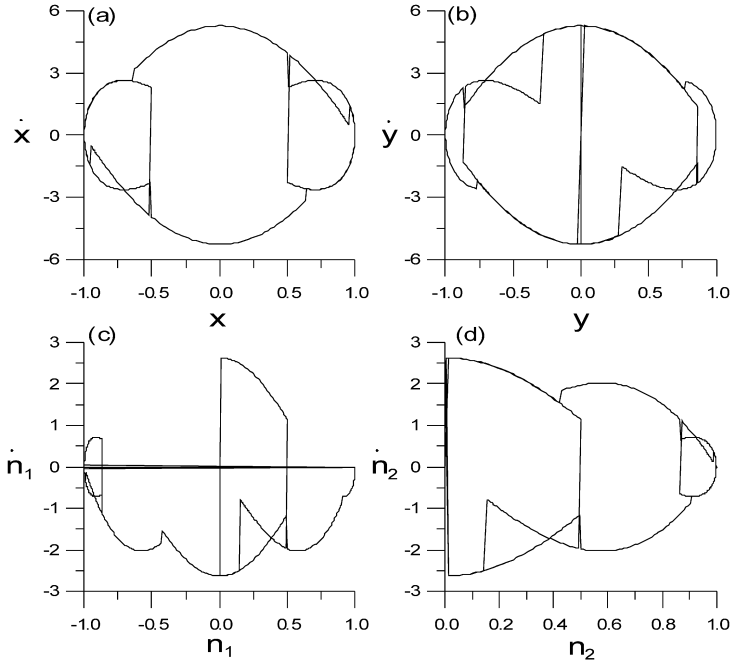

Fig. 6. The 1/3-subharmonic motion is shown through the phase portraits of (a) $(x, \dot{x})$, (b) $(y, \dot{y})$, (c) $(n_1, \dot{n}_1)$ and (d) $(n_2, \dot{n}_2)$.

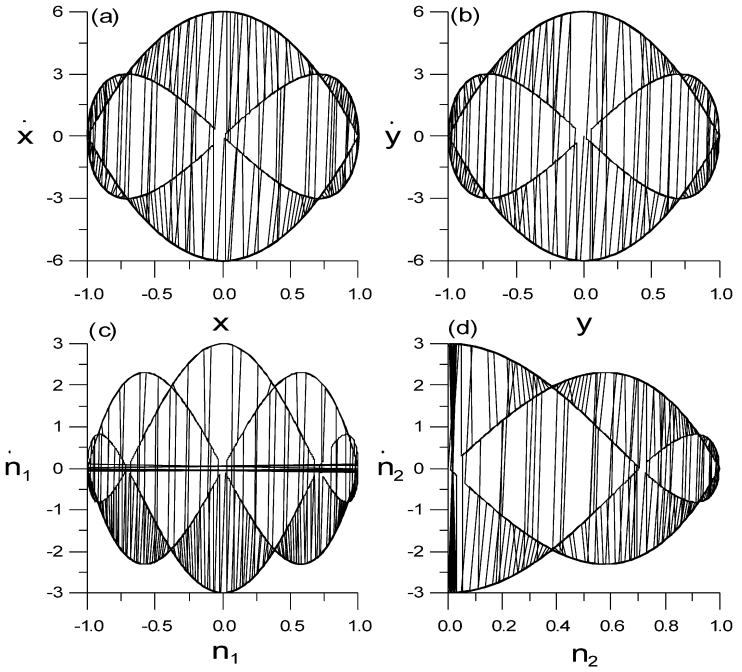

Fig. 7. A typical quasiperiodic motion is shown through the phase portraits of (a) $(x, \dot{x})$, (b) $(y, \dot{y})$, (c) $(n_1, \dot{n}_1)$ and (d) $(n_2, \dot{n}_2)$.

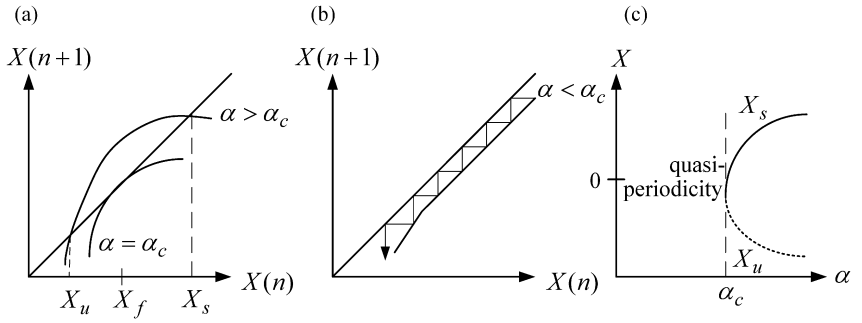

Fig. 8. The inverse tangent bifurcation occurs when α changes from $\alpha > \alpha_c$ to $\alpha < \alpha_c$. For the latter case when α is very close to α_c there happens a type I intermittency.

7. The phenomenon of intermittency

In Eq. (50) it is convenient to take $X(n) := \tan(\theta(n))$ as the new variable, such that

$$X(n+1) = F\big(X(n)\big), \tag{95}$$

$$F\big(X(n)\big) := \frac{G_{21} + G_{22}X(n) + G_{23}\sqrt{1+X^2(n)}}{G_{11} + G_{12}X(n) + G_{13}\sqrt{1+X^2(n)}}. \tag{96}$$

For this map by solving $F(X) = X$ we obtain two fixed points at $X = X_s$ and $X = X_u$ when $\alpha > \alpha_c$. The fixed point $X = X_u$ is unstable and $X = X_s$ is stable as schematically shown in Fig. 8(a). When α approaches to α_c from above the two fixed points (one stable and one unsta-

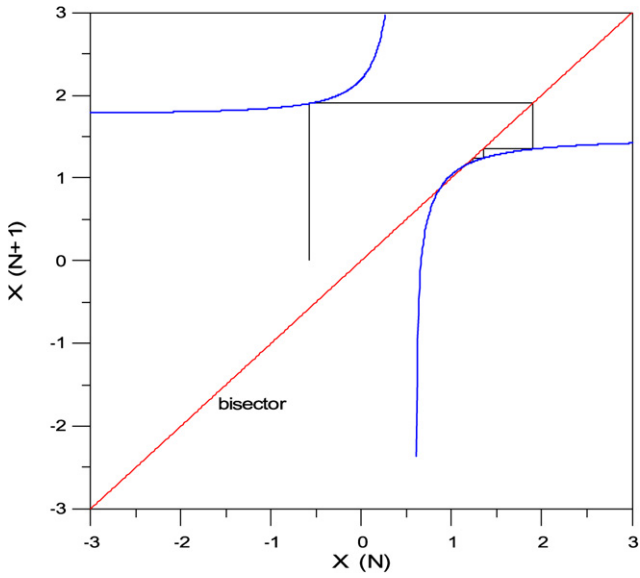

Fig. 9. For the case $\alpha = 1.77$ the iteration map is shown with the plot of $X(N+1)$ versus $X(N)$.

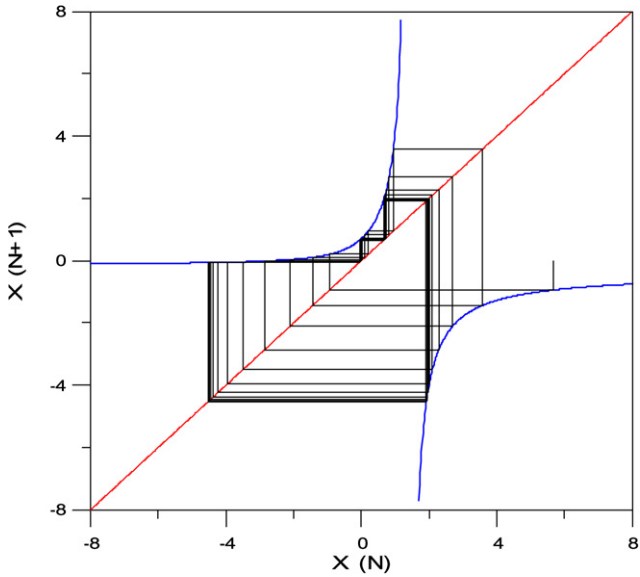

Fig. 10. For the case $\alpha = 1$ the iteration map is shown with the plot of $X(N+1)$ versus $X(N)$.

ble) merge together at $X = X_f$ as shown in Fig. 8(a), where X_f can be calculated by inserting $(x_f, y_f) = (\sqrt{2}/2, \sqrt{2}/2)$ into $X_f = y_f/x_f = 1$. When $\alpha < \alpha_c$ the map (95) has no fixed point, and the iteration map generated from it does not converge to any point.

In order to demonstrate these phenomena, let us consider the value $\alpha = 1.77 > \alpha_c$ as that used in Fig. 3, and plot the iteration map in Fig. 9. Starting from the initial value $X = -\tan\pi/6$ the orbit converges to the stable fixed point within only few steps. Next, we consider the value $\alpha = 1 < \alpha_c$ as that used in Fig. 4, and plot the iteration map in Fig. 10. Starting from the initial

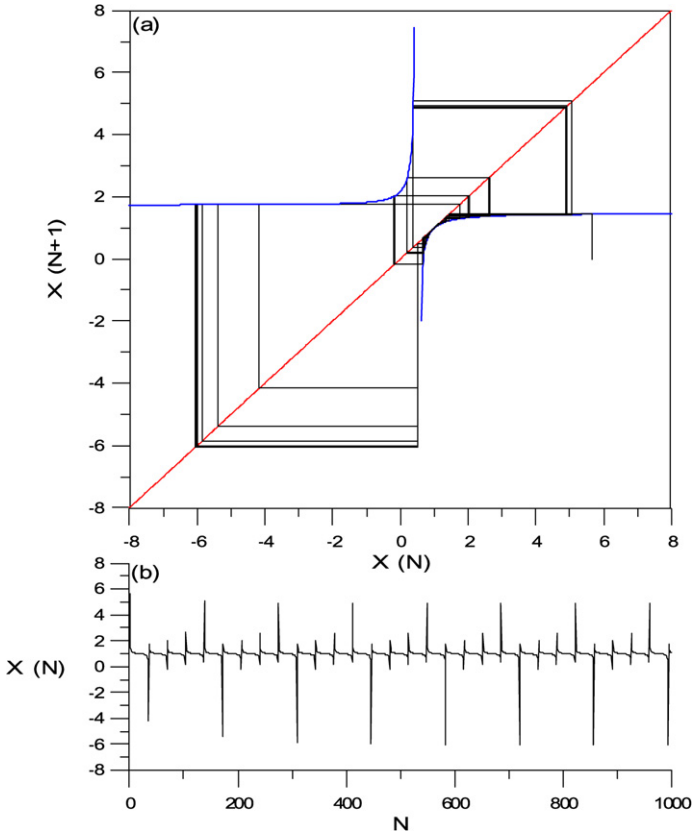

Fig. 11. For the case $\alpha = 1.762$ the iteration map is shown in (a) with the plot of $X(N+1)$ versus $X(N)$, and (b) the variation of $X(N)$ with respect to N. The intermittency of X appears.

value $X = \tan 4\pi/9$ the orbit does not converge to any point and continues to iterate on these two branch curves.

When the parameter α is kept very close to, but still less than α_c, the right branch curve of the map (95) comes very close to the bisector, but does not touch it, leaving thereby a very narrow corridor between the curve and the bisector as shown schematically in Fig. 8(b) and numerically in Fig. 11(a) for the case $\alpha = 1.762$. Therefore, there is an inverse tangent bifurcation when α varies from $\alpha > \alpha_c$ to $\alpha < \alpha_c$ as schematically shown in Fig. 8(c). Every time when one iterate point falls near the entrance to one of these corridors, it will take many iterations to pass through the corridor as shown in Fig. 11(a) for the case $\alpha = 1.762$. However, some sort of the memory of the fixed point at $X = X_f$ is displayed since the iteration slows down in the vicinity of $X = X_f$, and therefore as mentioned numerous steps are required to move through the narrow corridor between the curve and the bisector. When α is very close to α_c, this looks much like a segment of convergent iteration to the ghost fixed point $X = X_f$ at α_c and leads to a laminar phase of iteration as shown in Fig. 11(b). Having passed one corridor, the point makes a number of large-step jumps before falling again to the entrance of the corridor. These jumps constitute the random bursts of the irregular phase.

The intermittency can also be explored in terms of the map in Eq. (47). Under the same parameter value of $\alpha = 1.762$, we display the iteration trajectory of (x, y) in Fig. 12(a). The

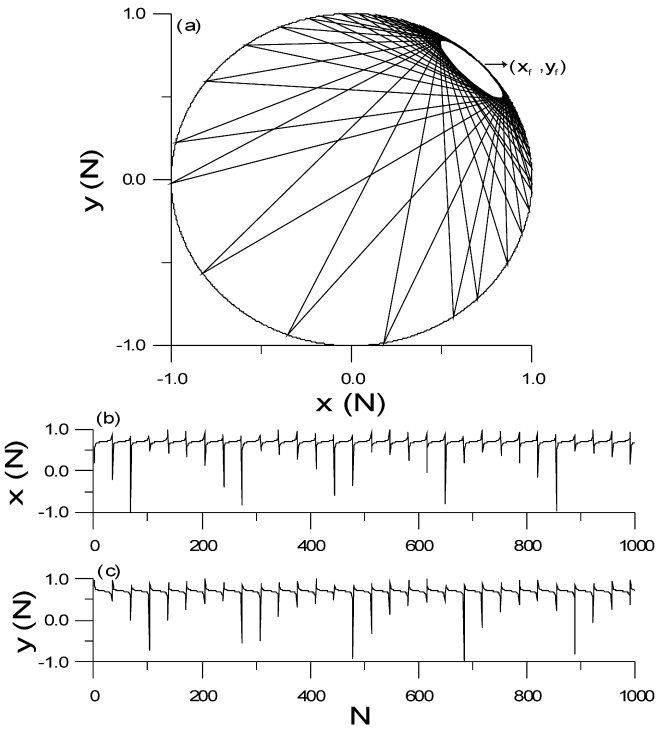

Fig. 12. For the case $\alpha = 1.762$ the iteration orbit of (x, y) is plotted in (a), and the variations of $x(N)$ and $y(N)$ with respect to N are plotted in (b) and (c). The intermittencies of x and y appear for this case.

lines connecting the points are used to stress the jump phenomena in the irregular phase. From this figure it can be seen that there is a very narrow corridor on the right-upper side near to the point (x_f, y_f). When the trajectory point enters this corridor it needs much more periods of time to pass this narrow tunnel and then leads to a laminar phase. Immediately after the trajectory leaves the corridor a great jump of the orbit may occur and then it is reinjected into the corridor from the other end to initiate a new regular phase. Figures 12(b) and 12(c) exhibit the intermittent phenomena of x and y.

8. Conclusions

Through a detailed study of Eq. (1) the characters of this equation were identified from several viewpoints: a quadratic differential equations system on $\mathbb{S}^1$, and a linear differential equations system in the Minkowski space $\mathbb{M}^3$. The symmetry groups are $PSO_o(2, 1)$ and $SO_o(2, 1)$. Under discontinuous periodic inputs with different amplitude the Poincaré maps were constructed, which led us being able to give a detailed bifurcation analysis. For larger values of α the responses are periodic, but below a critical value the inverse tangent bifurcation occurs and the responses become quasiperiodic or subharmonic depending on the value of n/m in Eq. (90) irrational or rational. The phenomenon of intermittency of the Poincaré circle map was pointed out and the mechanism of intermittency was also explored. We have shown a type I intermittency to the quasiperiodic motion under a discontinuous periodic input as that under a continuous periodic input on the circular differential equation discussed by Liu [6].

Acknowledgments

The author would like to acknowledge the constructive comments of anonymous referees and the editors to refine some arguments of this paper.

References

[1] J.K. Hale, H. Kocak, Dynamics and Bifurcations, Springer-Verlag, New York, 1991.
[2] H.-K. Hong, C.-S. Liu, Y.-P. Shiao, B.-C. Shih, Planar double-slip model for polycrystal plasticity and micro tension tests of pure nickel and copper, J. Eng. Mater. Tech. ASME 124 (2002) 314–321.
[3] C.V.A. Kumar, K.S. Kumar, T.R. Ramamohan, Chaotic dynamics of periodically forced spheroids in simple shear flow with potential application to particle separation, Rheo. Acta 34 (1995) 504–511.
[4] Y.A. Kuznetsov, Elements of Applied Bifurcation Theory, Springer-Verlag, New York, 1998.
[5] C.-S. Liu, Orientation control of particles and fibers for polymeric liquids and fiber reinforced materials, J. Chinese Inst. Engineers 20 (1997) 443–456.
[6] C.-S. Liu, Intermittent transition to quasiperiodicity demonstrated via a circular differential equation, Internat. J. Non-Linear Mech. 35 (2000) 931–946.
[7] C.-S. Liu, Cone of non-linear dynamical system and group preserving schemes, Internat. J. Non-Linear Mech. 36 (2001) 1047–1068.
[8] C.-S. Liu, The steady-state behavior of the Prandtl–Reuss material bifurcated under nonproportional circular strain paths, J. Chinese Inst. Engineers 26 (2003) 173–190.
[9] C.-S. Liu, Two-dimensional bilinear oscillator: group-preserving scheme and steady-state motion under harmonic loading, Internat. J. Non-Linear Mech. 38 (2003) 1581–1602.
[10] C.-S. Liu, Lie symmetries of finite strain elastic-perfectly plastic models and exactly consistent schemes for numerical integrations, Internat. J. Solids Structures 41 (2004) 1823–1853.
[11] C.-S. Liu, The asymptotic behavior of perfectly elastoplastic model under periodic square generalized strain paths, J. Chinese Inst. Engineers 28 (2005) 131–146.
[12] C.-S. Liu, H.-K. Hong, Spinor maps for symmetries in four dynamical systems, Internat. J. Appl. Math. 12 (2003) 307–356.
[13] C.-S. Liu, H.-K. Hong, D.-Y. Liou, Two-dimensional friction oscillator: Group-preserving scheme and handy formulae, J. Sound Vibration 266 (2003) 49–74.
[14] C.H. Menq, B.D. Yang, Non-linear spring resistance and friction damping of frictional constraint having two-dimensional motion, J. Sound Vibration 217 (1998) 127–143.
[15] Y. Pomeau, P. Manneville, Intermittent transition to turbulence in dissipative dynamical systems, Comm. Math. Phys. 74 (1980) 189–197.
[16] V.C. Prantil, J.T. Jenkins, P.R. Dawson, An analysis of texture and plastic spin for planar polycrystals, J. Mech. Phys. Solids 41 (1993) 1357–1382.
[17] H.G. Schuster, Deterministic Chaos: An Introduction, second ed., Physik-Verlag GmbH, Weinheim (F.R.G.), 1988.
[18] S.R. Strand, S. Kim, Dynamics and rheology of a dilute suspension of dipolar nonspherical particles in an external field: Part 1. Steady shear flows, Rheo. Acta 31 (1992) 94–117.
[19] G. Wang, S. He, A quantitative study on detection and estimation of weak signals by using chaotic Duffing oscillators, IEEE Trans. Circuits Syst. 50 (2003) 945–953.